J Therm Anal Calorim (2012) 110:685–694
DOI 10.1007/s10973-011-1901-2

Thermal analysis of cyclic carbonation behavior of CaO derived from carbide slag at high temperature

Yingjie Li · Hongling Liu · Rongyue Sun · Shuimu Wu · Chunmei Lu

Received: 13 July 2011 / Accepted: 30 August 2011 / Published online: 23 September 2011

Abstract In this work, CaO derived from the carbide slag (CaO–carbide slag) as a kind of typical industrial waste was used to capture CO_2 during the calcination/carbonation cycles. The carbonation kinetics and cyclic carbonation behavior of CaO–carbide slag were investigated in a thermogravimetric analyzer. The chemical reaction activation energy and the product layer diffusion activation energy for carbonation of CaO–carbide slag are 12.46 and 36.83 kJ mol^{-1}, respectively, which are significantly less than those for carbonation of CaO derived from the limestone (CaO–limestone). CaO–carbide slag shows higher carbonation conversion than CaO–limestone after enough reaction time and at the same number of cycles. Moreover, the calcination temperature and CO_2 concentration in the carbonation atmosphere have important effect on the carbonation behavior of CaO–carbide slag. The BET surface area of CaO–carbide slag is 1.6 times as large as that of CaO–limestone after 1 cycle and the average pore size of CaO–carbide slag is much smaller. In addition, the carbide slag contains much more Al_2O_3 than most of the limestones. These are reasons why carbide slag as a precursor can retain greater carbonation conversion than limestone in calcination/carbonation cycles.

Keywords Carbide slag · Calcination · Carbonation · Thermal analysis · CO_2 capture

Y. Li (✉) · H. Liu · R. Sun · S. Wu · C. Lu
School of Energy and Power Engineering, Shandong University, No. 17923 Jingshi Road, Jinan 250061, China
e-mail: liyj@sdu.edu.cn

Introduction

Carbon dioxide capture and storage (CCS) is a CO_2 abatement option that can contribute substantially to achieve ambitious CO_2 reduction targets. The electricity sector especially, with large point sources of CO_2, offers opportunities to apply CCS at a large scale. Results of techno-economic energy models show that power plants combined with CCS can indeed compete from a mitigation perspective with other non- or low-emitting CO_2 technologies such as nuclear energy or renewable energy [1].

There are many different CO_2 capture processes, however, their techno-economic feasibility for industrial applications must be seriously considered. Calcium looping technology is a promising new technique for high-temperature scrubbing of CO_2 from flue gas and syngas [2, 3] and current economic projections suggest it might be able to capture CO_2 at costs of ~$20/ton of avoided CO_2 [3]. The calcium looping technology, viz., calcium-based sorbent calcination/carbonation cycle using the reversible reaction between CaO and CO_2 was regarded to be encouraging to remove CO_2 [4] as shown in Fig. 1 and its applications including the pre-combustion CO_2 capture, e.g., sorption-enhanced hydrogen production process [5], hydrogen production by reaction-integrated novel gasification (HyPr-RING) [6] and the zero-emission carbon (ZEC) hydrogasification process [7], and post-combustion CO_2 capture [8] were reported in the literature.

Recently, lots of researchers paid more attention to investigate the CO_2 capture behavior of CaO derived from limestone and dolomite under the different reaction conditions [9–12] and study how to improve their the CO_2 capture capacity during the long-term calcination/carbonation cycles [3, 12, 13]. Moreover, the carbonation characteristics of CaO derived from the calcium-based sorbents

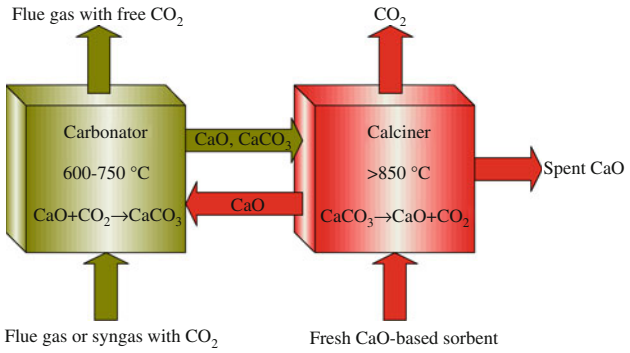

Fig. 1 Process scheme of the calcium looping technology for CO_2 capture

other than limestone or dolomite such as shell [14, 15] and oil shale ashes [16–18] at high temperature were also reported. However, the study on CO_2 capture behavior of calcium-based wastes generated from the industrial production in the calcium looping cycle has been barely reported.

Many calcium-based industrial wastes are produced in paper pulp plants and chlor-alkali plants in China every year. It is an interesting and challenging topic to recycle the industrial wastes to reduce environmental pollution and save valuable resources [19]. China produces the largest amount of calcium carbide (CaC_2) through reaction of calcined limestone (CaO) with coal char (C). About 70% of the ethyne gas (C_2H_2), which is the raw material of poly(vinyl chloride) (PVC), is produced from calcium carbide in China. About 1.5–1.9 tons of dried calcium carbide residue wastes are obtained in the production of 1 ton of PVC in a chlor-alkali plant [20]. The reaction mechanism is as follows

$$CaCO_3 \rightarrow CaO + CO_2 \quad (1)$$

$$CaO + 3C \rightarrow CaC_2 + CO \quad (2)$$

$$CaC_2 + 2H_2O \rightarrow C_2H_2 + Ca(OH)_2(\text{carbide slag}) \quad (3)$$

CaC_2 reacts with water to produce C_2H_2 gas and waste, viz., carbide slag which is mainly composed of $Ca(OH)_2$ [20]. And the carbide slag as a kind of calcium-based industrial waste is ordinarily landfilled outside the chlor-alkali plants. In this work, the carbide slag is used as a CO_2 sorbent during the calcination/carbonation cycles. It is expected to create a new way that combines calcium looping technology for CO_2 capture with calcium-based industrial wastes recycling.

Experimental

The carbide slag was sampled from a factory for polyvinyl chloride production by calcium carbide acetylene method in Shandong Province, China. A kind of typical limestone in Shandong province, China was employed to compare the CO_2 capture behavior with the carbide slag. The chemical components of the carbide slag and the limestone were analyzed by X-ray fluorescence (XRF) as shown in Table 1. The predominating constituent of the carbide slag is $Ca(OH)_2$ by XRD analysis. The particle size of the sorbent is below 0.125 mm.

The cyclic calcination/carbonation behavior of the sorbents with reaction time was studied in a thermogravimetric analyzer (TG). The mass of the sample in the TG is 10 ± 0.1 mg. The furnace temperature of TG increased to a calcination temperature 850–1000 °C with a heating rate of 30 °C min^{-1} and lasted 15 min at ultimate calcination temperature under pure N_2. And then the furnace temperature decreased to a carbonation temperature 600–700 °C from the calcination temperature under pure N_2. Then the reaction atmosphere was switch to carbonation atmosphere and the calcined sample was carbonated for 30 min. The first calcination/carbonation cycle of the sample was finished. 15% CO_2–85% N_2 gas mixture and 100% CO_2 atmosphere were chosen as the carbonation atmosphere, respectively. The cyclic carbonation conversion of the sample during the carbonation process was calculated by

$$X_N = \frac{m_{\text{carb},N}(t) - m_{\text{cal},N}}{m_0 \cdot b} \cdot \frac{W_{\text{CaO}}}{W_{\text{CO}_2}} \quad (4)$$

where X_N is carbonation conversion of sample with reaction time during Nth cycle. t is reaction time, s. m_0 is initial mass of sample, mg. b is content of CaO in initial sorbent, %. $m_{\text{carb},N}(t)$ is mass of carbonated sample with reaction time t during Nth cycle, mg. $m_{\text{cal},N}$ is mass of sample after complete calcination during Nth cycle, mg. W_{CaO} and W_{CO_2} are mole mass of CaO and CO_2, respectively, g mol^{-1}.

The surface morphology of CaO derived from the carbide slag and the limestone (CaO–carbide slag and CaO–limestone) after different cycles from TG was analyzed by field emission scan electron microscope (SEM). Micromeritics ASAP 2020-M nitrogen adsorption analyzer was used to analyze surface area and average pore size of CaO derived from the different precursor after 1 cycle. It should be mentioned that the surface area and average pore size were calculated by BET method and BJH model, respectively.

Results and discussion

Carbonation kinetics of CaO–carbide slag

Figure 2a shows the effect of carbonation temperature on the carbonation conversions of CaO–carbide slag and CaO–limestone during 1 cycle. The CaO derived from the

Table 1 Chemical components of carbide slag and limestone in wt%

Sample	CaO	MgO	SiO_2	Fe_2O_3	Al_2O_3	Na_2O	TiO_2	Others	LOI
Carbide slag	61.96	0.12	3.38	0.18	3.44	0.03	0.49	1.88	28.52
Limestone	52.08	1.32	3.32	0.03	0.53	0.02	–	0.47	42.23

two sorbents both reaches higher carbonation conversion at 700 °C. At the same carbonation temperature, the carbonation conversion of CaO–carbide slag is lower than that of CaO–limestone before a certain time, but the situation is converse after that time. The carbonation rate of the sorbent is calculated by

$$r_1 = \frac{\mathrm{d}X_1}{\mathrm{d}t} \tag{5}$$

where r_1 is carbonation rate of the sorbent at t during the first carbonation, s^{-1}. The carbonation rates of CaO derived from the sorbents at the different carbonation temperatures during 1 cycle are depicted in Fig. 2b. The carbonation rate integrates the chemical reaction rate and the gas diffusion rate. The maximum carbonation rate of CaO–carbide slag is smaller than that of CaO–limestone at the same carbonation temperature. It is observed that CaO–carbide slag needs longer time to achieve the maximum carbonation rate. Although carbonation rate of CaO–limestone is greater than that of CaO–carbide slag at the initial reaction stage and under the same reaction conditions, the situation is also converse after a time. The variety of the carbonation rates of the two sorbents with the reaction time agrees with that of their carbonation conversions. It is found that the carbonation rate of CaO–limestone at 700 °C is lower than that at 650 °C before 300 s and the situation is converse after 300 s. It may be attributed to a difference in particle size distribution between the samples of the limestone at the 650 and 700 °C. Although the particle size of all the samples is below 0.125 mm, they have still the difference in particle size distribution and average particle size. The small difference in average particle size would result in a difference in carbonation reaction. Bhatia and Perlmutter [21] reported the carbonation behavior of CaO–limestone at the different carbonation temperatures in the TG and found the similar phenomenon. The carbonation kinetics of CaO–carbide slag and CaO–limestone can be calculated according to the effect of the carbonation temperature on the carbonation conversion during 1 cycle.

The shrinking unreacted core model was usually used to describe the gas–solid reaction [22–26]. The CaO is thought to be consisting of numerous solid particles which are considered to be small but dense grains. Therefore, in this work the shrinking unreacted core model is employed to simulate carbonation reaction of CaO–carbide slag with the reaction time and analyze its carbonation kinetics

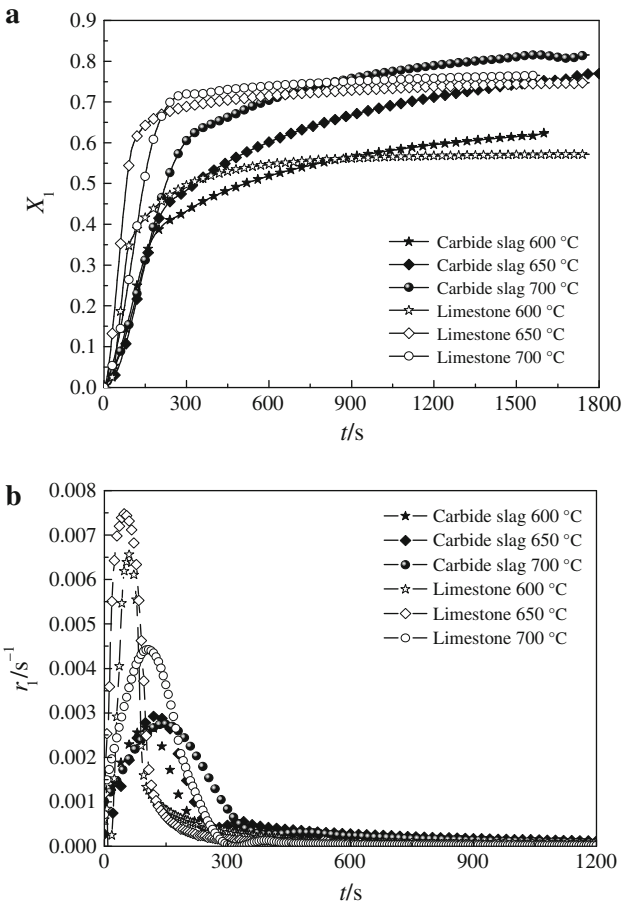

Fig. 2 Effect of carbonation temperature on carbonation conversions and carbonation rates of CaO derived from carbide slag and limestone during 1 cycle (calcination temperature 850 °C, carbonation atmosphere 15% CO_2/85% N_2). **a** Carbonation conversion and **b** carbonation rate

during 1 cycle. And the difference between CaO–carbide slag and CaO–limestone in carbonation kinetics is also compared. The carbonation reaction initiates on the grain surface in the early stage which is called the chemical-reaction-controlled stage. A layer of $CaCO_3$ products is formed around each CaO grain that separates the reaction surface of the solid from gas reactant with the reaction going on. The CO_2 have to diffuse through the product layer to the reaction surface. And then the carbonation reaction shifts to the product-layer-diffusion-controlled stage [27, 28].

The model in this investigation assumes negligible mass transfer through the gas film and isothermal conditions in

the reactor. If the chemical reaction is the rate-limiting step, the relationship between the reaction time and the carbonation conversion is given as [28]

$$t = AG(X_1) \tag{6}$$

$$A = \frac{\rho_p R_p}{\alpha k C_{A0}} \tag{7}$$

If the diffusion through the product layer is the rate-limiting step, the relationship is shown as follows:

$$t = BP(X_1), \tag{8}$$

$$B = \frac{\rho_p R_p^2}{6\alpha D_s C_{A0}} \tag{9}$$

where A and B is parameters in Eqs. 6 and 8, min; $G(X_1)$ and $P(X_1)$ is function defined by Eqs. 6 and 8, dimensionless; ρ_p is sorbent density, 0.059 g cm^{-3}; R_p is average radius of unreacted core for CaO particle, cm; k is kinetic parameters, cm s^{-1}; C_{A0} is concentration of CO_2, 6.7 × 10^{-7} mol cm^{-3}; D_s is effective diffusivity, cm^2 s^{-1}; α is stoichiometric coefficient of solid reactant, $\alpha = 1$. $G(X_1)$ and $P(X_1)$ are two functions related to the sulfation conversion as follows [28]

$$G(X_1) = 1 - (1 - X_1)^{1/3} \tag{10}$$

$$P(X_1) = 1 - 3(1 - X_1)^{2/3} + 2(1 - X_1) \tag{11}$$

k and D_s can be calculated according to Arrhenius' law by

$$k = k_0 \exp\left(-\frac{E_a}{RT}\right) \tag{12}$$

$$D_s = D_0 \exp\left(-\frac{E_p}{RT}\right) \tag{13}$$

where k_0 is pre-exponential factor, cm s^{-1}; D_0 is effective diffusivity at external grain surface, cm^2 s^{-1}; E_a is chemical reaction activation energy, kJ mol^{-1}; E_p is activation energy for product layer diffusion, kJ mol^{-1}; R is gas constant, 8.314 J mol^{-1} K^{-1}; T is carbonation temperature, K.

Incorporating Eqs. 7 and 9, we get the new equations by taking the logarithm of both sides in Eqs. 12 and 13 as follows:

$$\ln\frac{1}{A} = \ln k_0 + \ln\frac{C_{A0}}{\rho_p R_p} - \frac{E_a}{RT} \tag{14}$$

$$\ln\frac{1}{B} = \ln D_0 + \ln\frac{6C_{A0}}{\rho_p R_p^2} - \frac{E_p}{RT} \tag{15}$$

The physical property parameters such as ρ_p, R_p are assumed constant at the different carbonation temperatures. The shrinking unreacted core model is determined by k_0, E_a, D_0, and E_p in different reaction stages, so these parameters for the carbide slag and the limestone must be calculated according to the experiment data.

Plots of $G(X_1) - t$ and $P(X_1) - t$ for carbonation reaction of CaO–carbide slag and CaO–limestone are shown in Figs. 3 and 4, respectively. And the solid lines obtained from linear fitting refer to the slopes of $G(X_1) - t$ and $P(X_1) - t$. The correlation coefficients for the linear fits of $G(X_1) - t$ are between 0.979 and 0.998, and those of $P(X_1) - t$ are between 0.997 and 0.999. It indicates that the shrinking unreacted core model is appropriate to describe the carbonation kinetics of CaO–carbide slag and CaO–limestone. A and B are the slope coefficients of the fitting lines for $G(X_1) - t$ and $P(X_1) - t$, so they are easily determined. Figure 5 exhibits ln $1/A - 1/T$ and ln $1/B - 1/T$ for CaO derived from the two sorbents which are related linearly, respectively.

k_0, E_a, D_0, and E_p can be all calculated according to the data in Fig. 5 and they are demonstrated in Table 2. The E_a and E_p for carbonation of CaO–limestone are 36.71 and 99.31 kJ mol^{-1}. Sun et al. [27] and Dedman and Owen [29] reported that the E_a for carbonation of CaO–limestone was 29 ± 4 and 39.71 ± 8.36 kJ mol^{-1}, respectively. These results are similar. The E_a and E_p for carbonation of

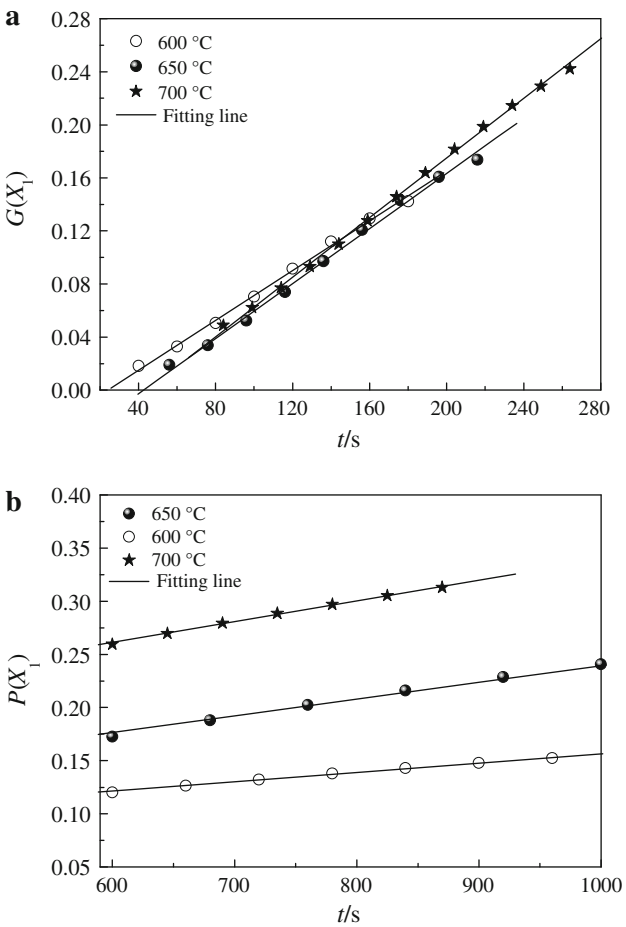

Fig. 3 Plots of the function G(X_1) and P(X_1) vs. t for CaO derived from carbide slag during 1 cycle. **a** G(X_1) vs. t and **b** $P(X_1)$ vs. t

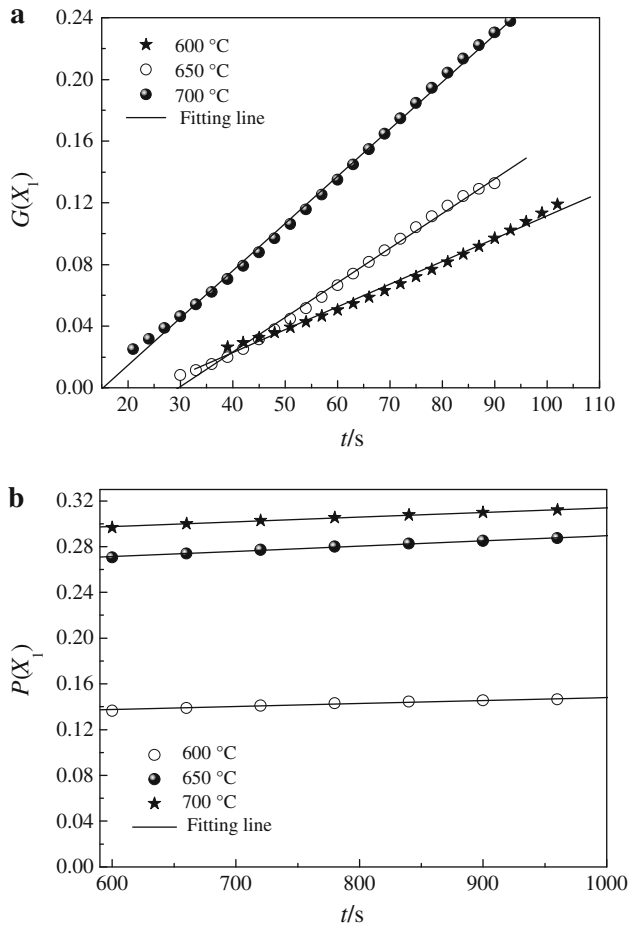

Fig. 4 Plots of the function $G(X_1)$ and $P(X_1)$ vs. t for CaO derived from limestone during 1 cycle. **a** $G(X_1)$ vs. t and **b** $P(X_1)$ vs. t

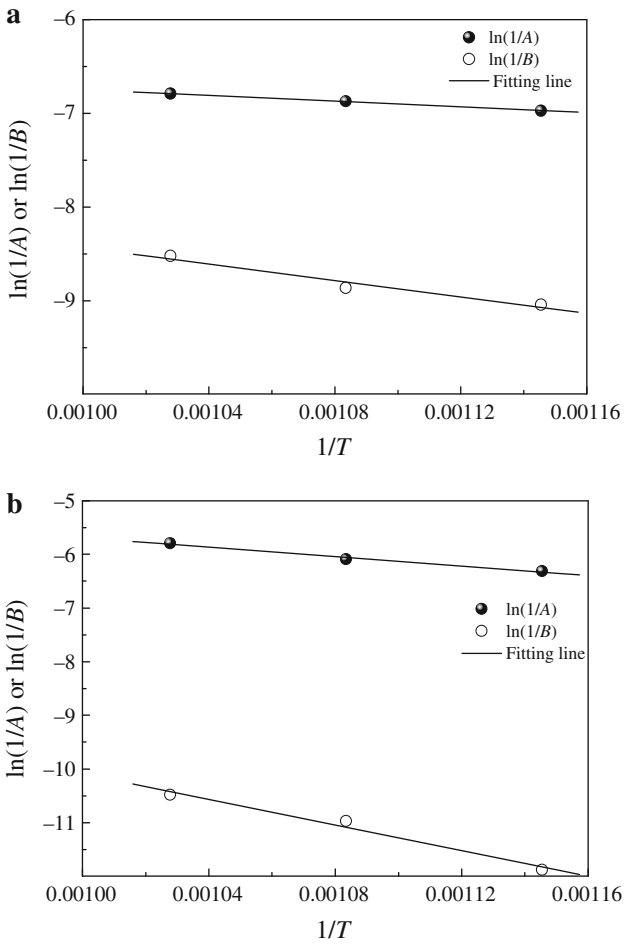

Fig. 5 Arrhenius graph for carbonation reaction of CaO derived from carbide slag and limestone. **a** CaO derived from carbide slag and **b** CaO derived from limestone

CaO–carbide slag are 12.46 and 36.83 kJ mol^{-1}. The carbonation reaction of CaO–carbide slag seems more easily proceeds than that of CaO–limestone.

Effect of cycle number on carbonation behavior of CaO–carbide slag

Figures 6 and 7 exhibit the carbonation conversion for CaO–carbide slag and CaO–limestone with the reaction time during the different cycles, respectively. The cyclic carbonation conversion of CaO–limestone increases rapidly with the reaction time, but after 198 s the conversion keeps a slow increase. However, the cyclic carbonation conversion of CaO–carbide slag still increases more rapidly than that of CaO–limestone after 192 s. The carbonation conversions of CaO–carbide slag and CaO–limestone both decrease with the number of cycles, but the decay in the conversion of CaO–limestone is more serious than that of CaO–carbide slag. CaO–carbide slag shows higher carbonation conversion after enough reaction time and after the same number of cycles. For example, the carbonation conversions of CaO–carbide slag and CaO–limestone after 1 cycle at 1500 s are 0.81 and 0.76, respectively. Moreover, the carbonation conversion of CaO–carbide slag is 1.8 times as high as that of CaO–limestone after 10 cycles and at 1500 s.

Effect of calcination temperature on carbonation behavior of CaO–carbide slag

Figure 8 shows the effect of calcination temperature on cyclic carbonation conversion of CaO–carbide slag. Higher calcination temperature maybe aggravates readily sintering of calcium-based sorbents. And the sintering is responsible for the decay in the carbonation conversions of the sorbents, because it induces the blockage of lots of pores in the sorbents [30]. After 1 cycle and at 1600 s, the carbonation conversion of CaO–carbide slag exhibits a drop by 31% with increasing the calcination temperature from 850 to 1000 °C. In addition, the conversion of CaO–carbide slag after 10 cycles and at 1600 s decreases by 48%

Table 2 Activation energy and pre-exponential factor

Sample	E_a/kJ mol^{-1}	k_0/cm s^{-1}	E_p/kJ mol^{-1}	D_0/cm^2 s^{-1}
Carbide slag	12.46	0.12	36.83	4.08×10^{-4}
Limestone	36.71	6.21	99.31	0.14

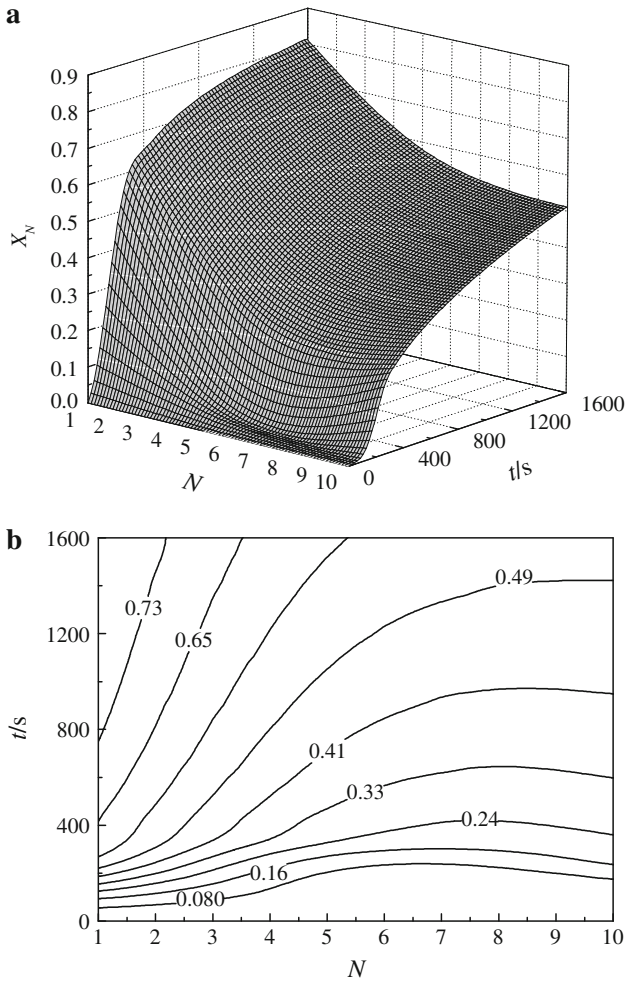

Fig. 6 Cyclic carbonation conversions of CaO derived from carbide slag with reaction time (calcination temperature 850 °C, carbonation temperature 700 °C, and carbonation atmosphere 15% CO_2/85% N_2). **a** Surface plot and **b** contour plot

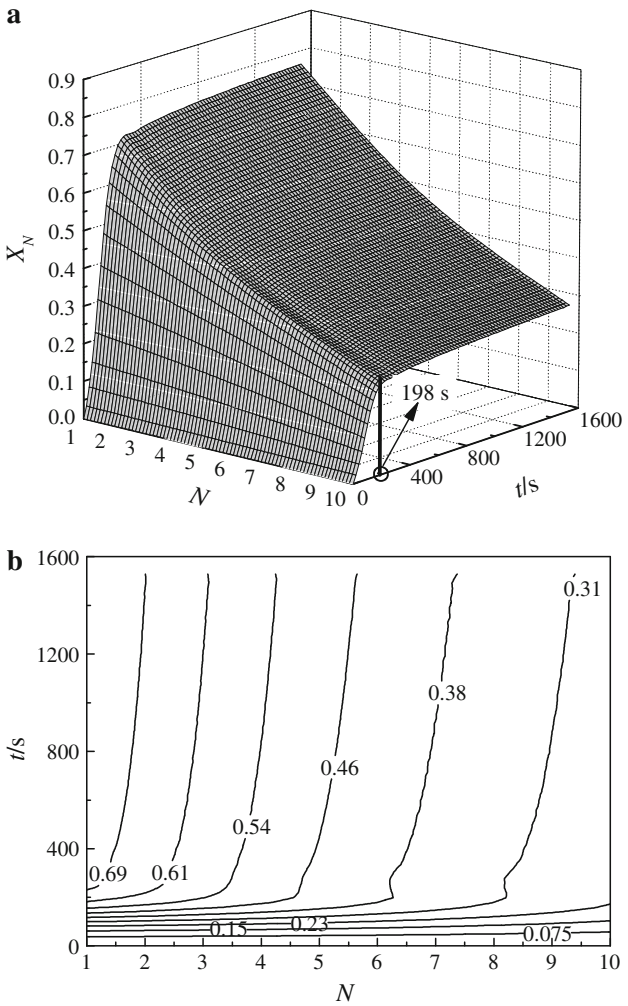

Fig. 7 Cyclic carbonation conversions of CaO derived from limestone with reaction time (calcination temperature 850 °C, carbonation temperature 700 °C, and carbonation atmosphere 15% CO_2/85% N_2). **a** Surface plot and **b** contour plot

when calcination temperature increasing from 850 to 1000 °C. Grasa and Abanades [31] reported that CaO–limestone after 10 cycles for calcination at 1000 °C achieved a carbonation conversion of 0.14 and they thought that calcination temperature above 950 °C and long calcination time accelerated the decay in CO_2 capture capacity of CaO–limestone. When the calcination temperature is 1000 °C, the carbonation conversion of CaO–carbide slag after 10 cycles and at 1600 s is about 0.26 which is almost twice as high as that of CaO–limestone reported by Grasa and Abanades [31]. It reveals that CaO–carbide slag still retains higher cyclic CO_2 capture capacity at the high calcination temperature above 950 °C.

Effect of carbonation atmosphere on carbonation behavior of CaO–carbide slag

The carbonation conversions of CaO–carbide slag under different carbonation atmospheres containing 100% CO_2 and 15% CO_2 concentration are depicted in Fig. 9a. Before 300 s, the carbonation conversion of CaO–carbide slag increases with the CO_2 concentration increasing from 15 to

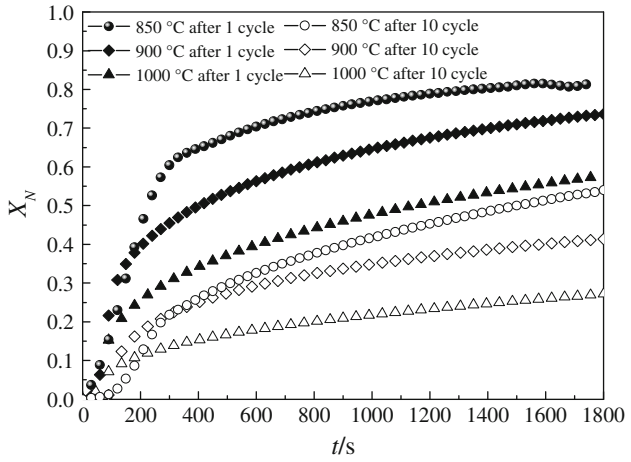

Fig. 8 Effect of calcination temperature on cyclic carbonation conversions of CaO derived from carbide slag (carbonation temperature 700 °C, carbonation atmosphere 15% CO_2/85% N_2)

100%. However, after 300 s, the carbonation conversions at different CO_2 concentration in the carbonation atmosphere are almost the same. Figure 9b shows the effect of CO_2 concentration in the carbonation atmosphere on the carbonation rate of CaO–carbide slag. The carbonation rate of CaO–carbide slag under 100% CO_2 atmosphere increases more rapidly with the reaction time than that under 15% CO_2–85% N_2 gas mixture. The maximum carbonation rate of CaO for carbonation under 100% CO_2 atmosphere is approximately twelve times as high as that under 15% CO_2–85% N_2 gas mixture. After 300 s, the carbonation rate of CaO–carbide slag under 100% CO_2 atmosphere is almost identical to that under 15% CO_2–85% N_2 gas mixture. The carbonation reaction of CaO–carbide slag in 300 s is mainly in the chemical-reaction-controlled stage. It reveals that the CO_2 concentration in the carbonation atmosphere has an important effect on the carbonation behavior of CaO–carbide slag in the chemical-reaction-controlled stage, but it has no noticeable effect on the carbonation in the product-layer-diffusion-controlled stage.

Microstructure analysis

Figure 10 shows the SEM micrographs of CaO–carbide slag and CaO–limestone after 1 and 10 cycles. The surface of CaO–carbide slag appears more porous than that of CaO–limestone after 1 cycle as seen in Figs. 10a and b. After 10 cycles, CaO–carbide slag still seems loose and expansive, as presented in Fig. 10c. The surface of CaO–limestone after 10 cycles appears compact and becomes an agglomeration due to sintering as shown in Fig. 10d. It is apparent that the structure of CaO–carbide slag is beneficial to carbonation and CO_2 diffusion in the particle. That is a reason why CaO–carbide slag possesses higher CO_2 capture capacity than CaO–limestone during the cycles.

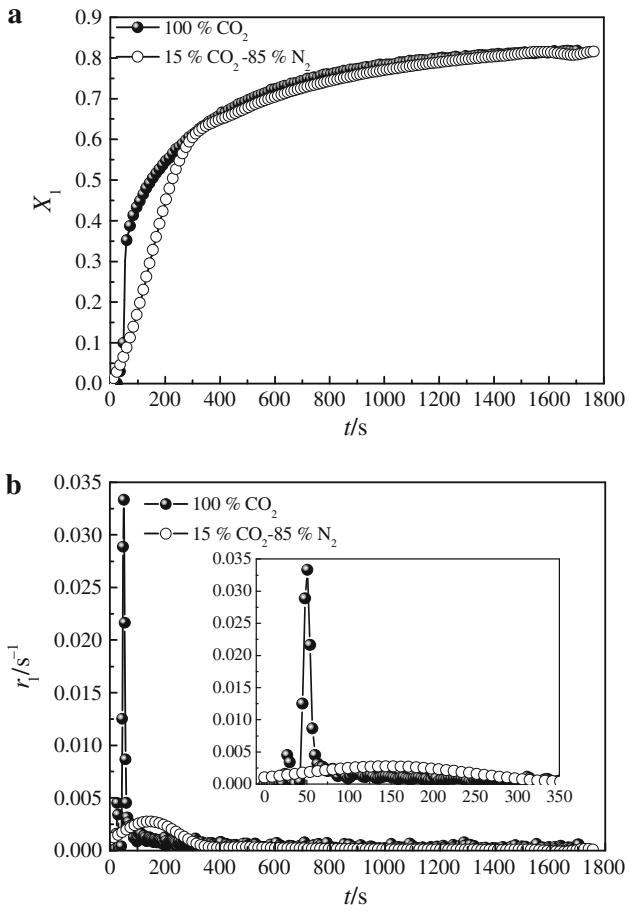

Fig. 9 Effect of carbonation atmosphere on carbonation conversion and rate of CaO derived from carbide slag after 1 cycle (calcination temperature 850 °C, carbonation temperature 700 °C). **a** Carbonation conversion and **b** carbonation rate

The BET surface area and the average pore size of CaO–carbide slag and CaO–limestone after 1 cycle are shown in Table 3. The BET surface area of CaO–carbide slag is 1.6 times as large as that of CaO–limestone after 1 cycle. Larger surface area of the calcines is more reactive for gas–solid reaction [32, 33]. It is found that the average pore size of CaO–carbide slag is obviously smaller than that of CaO–limestone. Smaller pore size results in larger surface area of the sorbent. Since CaO–carbide slag holds larger surface area and smaller average pore size, it retains higher CO_2 capture capacity during the multiple calcination/carbonation cycles.

Comparison between cyclic carbonation conversions for CaO derived from different precursors

The test on 20 calcination/carbonation cycles for CaO–carbide slag was done in the TG (reaction condition: carbonation time 20 min, calcination temperature 850 °C, carbonation temperature 700 °C and carbonation

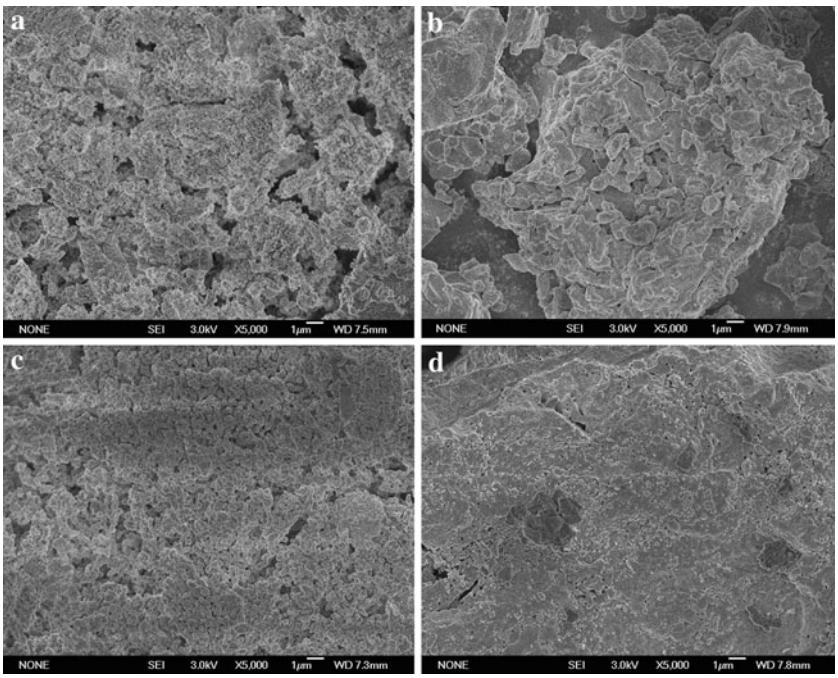

Fig. 10 SEM images of CaO derived carbide slag and limestone after 1 and 10 cycles (calcination temperature 850 °C, carbonation temperature 700 °C, and carbonation atmosphere 15% CO_2/85% N_2). **a** CaO derived carbide slag after 1 cycle, **b** CaO derived from limestone after 1 cycle, **c** CaO derived carbide slag after 10 cycles, and **d** CaO derived from limestone after 10 cycles

Table 3 BET surface area and average pore size of CaO derived from the different precursors after 1 cycle

Precursor	BET surface area/m^2 g^{-1}	Average pore size/nm
Carbide slag	17.19	8.7
Limestone	10.81	43.6

atmosphere 15% CO_2/85% N_2). The cyclic carbonation conversions of CaO–carbide slag were compared with those of CaO–limestone and CaO derived from dolomite (CaO–dolomite) reported in the references, as presented in Fig. 11. Those experiments reported by researchers [31, 34–36] were performed in the TG or fixed-bed reactor and reaction condition was similar to that in our work. It is observed that the cyclic carbonation conversion of CaO–carbide slag is lower than that of CaO–dolomite reported by Lisbona et al. [34] during previous 8 cycles, whereas, the conversion of the former is higher than that of the latter after 9 cycles. Moreover, the carbonation conversion of CaO–carbide slag is 1.4 times as high as that of CaO–dolomite after 20 cycles. Grasa and Abanades [31], Salvador et al. [35], and Abanades and Alvarez [36] reported the carbonation behaviors of CaO derived from the different limestones as shown in Fig. 11. In addition, Grasa and Abanades [31] summarized the carbonation conversion of the generic limestone with the number of cycles based on lots of tests, which is represented by a solid line in Fig. 11. It is seen that CaO–carbide slag exhibits a greater carbonation conversion than that of CaO derived from the different limestones during 20 cycles. As is mentioned above, the difference in the microstructure between CaO–carbide slag and CaO–limestone possibly

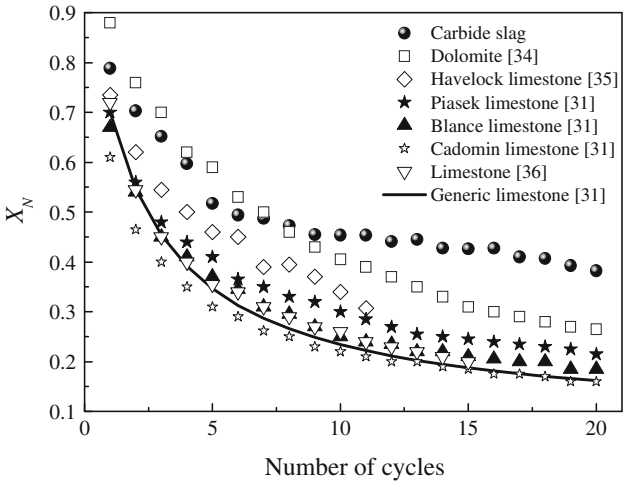

Fig. 11 Comparison between cyclic carbonation conversions of CaO derived from different precursors

results in a difference in the carbonation conversion between them. Moreover, the impurities other than CaO in CaO-based sorbents have also an effect on their carbonation conversions. It is observed from Table 1 that there is an obvious difference in the amount of Al_2O_3 between the carbide slag and the limestone (amount of Al_2O_3 in most of limestones reported is less than 1 wt%). It was reported that the presence of Al_2O_3 in the CaO-based sorbents could improve their anti-sintering performances and CO_2 capture capacities during the multiple calcination/carbonation cycles [12, 13]. Therefore, it may be another reason why CaO–carbide slag has higher carbonation conversion. The results show that the carbide slag seems promising as a CO_2 sorbent.

Conclusions

In this work, the shrinking unreacted core model was employed to simulate carbonation reaction of CaO–carbide slag during 1 cycle. The chemical reaction activation energy and the product layer diffusion activation energy for carbonation of CaO–carbide slag are obviously less than those for carbonation of CaO–limestone, respectively. Lower activation energy is beneficial to carbonation reaction and CO_2 diffusion through the product layer. The carbonation conversions of the CaO–carbide slag and CaO–limestone both decrease with the number of cycles, but the decrease in the conversion of the former is slower than that of the latter. CaO–carbide slag shows higher carbonation conversion after enough reaction time and at the same number of cycles. CaO–carbide slag still retains high cyclic CO_2 capture capacity at high calcination temperature above 950 °C. The CO_2 concentration in the carbonation atmosphere has an important effect on the carbonation behavior of CaO–carbide slag in the chemical-reaction-controlled stage, but it has no noticeable effect on the carbonation in the product-layer-diffusion-controlled stage. Since CaO–carbide slag holds larger surface area, smaller average pore size and more Al_2O_3, it retains higher CO_2 capture capacity during the multiple cycles. It indicates that the carbide slag seems promising as a CO_2 sorbent.

Acknowledgements Financial support from National Natural Science Foundation of China (51006064) is gratefully appreciated.

References

1. van den Broek M, Hoefnagels R, Rubin E, Turkenburg W, Faaij A. Effects of technological learning on future cost and performance. Prog Energy Combust Sci. 2009;35:457–80.
2. Dean CC, Blamey J, Florin NH, Al-Jeboori MJ, Fennell PS. The calcium looping cycle for CO_2 capture from power generation, cement manufacture and hydrogen production. Chem Eng Res Des. 2011;89:836–55.
3. Anthony EJ. Ca looping technology: current status, developments and future directions. Greenhouse Gas Sci Technol. 2011;1:36–47.
4. Anthony EJ. Solid looping cycles: a new technology for coal conversion. Ind Eng Chem Res. 2008;47:1747–54.
5. Harrison DP. Sorption-enhanced hydrogen production: a review. Ind Eng Chem Res. 2008;47:6486–501.
6. Lin SY, Suzuki Y, Hatano H, Harada M. Developing an innovative method, HyPr-RING, to produce hydrogen from hydrocarbons. Energy Convers Manage. 2002;43:1283–90.
7. Perdikaris N, Panopoulos KD, Fryda L, Kakaras E. Design and optimization of carbon-free power generation based on coal hydrogasification integrated with SOFC. Fuel. 2009;88:1365–75.
8. Charitos A, Hawthorne C, Bidwe AR, Korovesis L, Schuster A, Scheffknecht G. Hydrodynamic analysis of a 10 kWth calcium looping dual fluidized bed for post-combustion CO_2 capture. Powder Technol. 2010;200:117–27.
9. Chrissafis K. Multicyclic study on the carbonation of CaO using different limestones. J Therm Anal Calorim. 2007;89:525–9.
10. Chrissafis K, Paraskevopoulos KM. The effect of sintering on the maximum capture efficiency of CO_2 using a carbonation/calcination cycle of carbonate rocks. J Therm Anal Calorim. 2005;81:463–8.
11. Chrissafis K, Dagounaki C, Paraskevopoulos KM. The effects of procedural variables on the maximum capture efficiency of CO_2 using a carbonation/calcination cycle of carbonate rocks. Thermochim Acta. 2005;428:193–8.
12. Blamey J, Anthony EJ, Wang J, Fennell PS. The calcium looping cycle for large-scale CO_2 capture. Prog Energy Combust Sci. 2010;36:260–79.
13. Manovic V, Anthony EJ. Lime-based sorbents for high-temperature CO_2 capture—a review of sorbent modification methods. Int J Environ Res Pub Health. 2010;7:3129–40.
14. Ives M, Mundy RC, Fennell PS, Davidson JF, Dennis JS, Hayhurst AN. Comparison of different natural sorbents for removing CO_2 from combustion gases, as studied in a bench-scale fluidized bed. Energy Fuels. 2008;22:3852–7.
15. Li YJ, Zhao CS, Chen HC, Duan LB, Chen XP. CO_2 capture behavior of shell during calcination/carbonation cycles. Chem Eng Technol. 2009;32:1176–82.
16. Trikkel A, Keelmann M, Kaljuvee T. CO_2 and SO_2 uptake by oil shale ashes: effect of pre-treatment on kinetics. J Therm Anal Calorim. 2010;99:763–9.
17. Kaljuvee T, Toom M, Trikkel A, Kuusik R. Reactivity of oil shale ashes in the binding of SO_2. J Therm Anal Calorim. 2007;88:51–8.
18. Kaljuvee T, Trikkel A, Kuusik R. Decarbonization of natural lime-containing materials and reactivity of calcined products towards SO_2 and CO_2. J Therm Anal Calorim. 2001;64:1229–40.
19. Li YJ, Sun RY, Zhao JL, Han KH, Lu CM. Sulfation behavior of white mud from paper manufacture as SO_2 sorbent at fluidized bed combustion temperatures. J Therm Anal Calorim. 2011. doi: 10.1007/s10973-011-1537-2.
20. Cheng J, Zhou JH, Liu JZ, Cao XY, Cen KF. Physicochemical characterizations and desulfurization properties in coal combustion of three calcium and sodium industrial wastes. Energy Fuels. 2009;23:2506–16.
21. Bhatia SK, Perlmutter DD. Effect of the product layer on the kinetics of the CO_2-lime reaction. AIChE J. 1983;29:79–86.
22. Stanmore BR, Gilot P. Review—calcination and carbonation of limestone during thermal cycling for CO_2 sequestration. Fuel Process Technol. 2005;86:1707–43.
23. Anthony EJ, Granatstein DL. Sulfation phenomena in fluidized bed combustion systems. Prog Energy Combust Sci. 2001;27:215–36.
24. Li RY, Qi HY, You CF, Xu XC. Kinetic model of CaO/fly ash sorbent for flue gas desulphurization at moderate temperatures. Fuel. 2007;86:785–92.
25. Mohamed AR. Kinetic model for the reaction between SO_2 and coal fly ash/CaO/$CaSO_4$ sorbent. J Therm Anal Calorim. 2005;79:691–5.
26. Wieczorek-Ciurowa K. Peculiarities of interactions in the $CaCO_3$/CaO–SO_2/SO_3–air system. J Therm Anal Calorim. 1998;53:649–58.
27. Sun P, Grace JR, Lim CJ, Anthony EJ. Determination of intrinsic rate constants of the CaO–CO_2 reaction. Chem Eng J. 2007;63:47–56.
28. Wu ZH, Kou P, Yu ZW. The modulation of desulphurization properties of calcium oxide by alkali carbonates. J Therm Anal Calorim. 2002;67:745–50.
29. Dedman AJ, Owen AJ. Calcium cyanide synthesis. Part 4—the reaction $CaO + CO_2 = CaCO_3$. Trans Faraday Soc. 1962;58:2027–35.

30. Manovic V, Charland JP, Blamey J, Fennell PS, Lu DY, Anthony EJ. Influence of calcination conditions on carrying capacity of CaO-based sorbent in CO_2 looping cycles. Fuel. 2009;88:1893–900.
31. Grasa GS, Abanades JC. CO_2 capture capacity of CaO in long series of carbonation/calcination cycles. Ind Eng Chem Res. 2006;45:8846–51.
32. Liu B, Thomas PS, Ray AS, Guerbois JP. A TG analysis of the effect of calcination conditions on the properties of reactive magnesia. J Therm Anal Calorim. 2007;88:145–9.
33. Fennell PS, Paccinani R, Dennis JS, Davidson JF, Hayhurst AN. The effects of repeated cycles of calcinations and carbonation on a variety of different limestones, as measured in a hot fluidized bed of sand. Energy Fuels. 2007;21:2072–81.
34. Lisbona P, Martinez A, Lara Y, Remeo LM. Integration of carbonate CO_2 capture cycle and coal-fired power plants. A comparative study for different sorbents. Energy Fuels. 2010;24:728–36.
35. Salvador C, Lu D, Anthony EJ, Abanades JC. Enhancement of CaO for CO_2 capture in an FBC environment. Chem Eng J. 2003;96:187–95.
36. Abanades JC, Alvarez D. Conversion limits in the reaction of CO_2 with lime. Energy Fuels. 2003;17:308–15.